Characterising forest gap fraction with terrestrial lidar and photography: An examination of relative limitations

Steven Hancock, Richard Essery, Tim Reid, Joel Carle,
Robert Baxter, Nick Rutter, Brian Huntley

Published in Agricultural and Forest Meteorology, v 189, p 105-114, 2014

Abstract

Previous studies have shown that terrestrial lidar is capable of characterising forest canopies but suggest that lidar underestimates gap fraction compared to hemispherical camera photography. This paper performs a detailed comparison of lidar to camera-derived gap fractions over a range of forest structures (in snow affected areas) and reasons for any disagreements are analysed.

A terrestrial laser scanner (Leica C10 first return system) was taken to Abisko in Northern Sweden (sparse birch forests) and Sodankylä in Finland (spruce and pine forests) where five plots of varying density were scanned at each (though one Abisko plot was rejected due to geolocation issues). Traditional hemispherical photographs were taken and gap fraction estimates compared.

It is concluded that, for the sites tested, the reported underestimates in gap fraction can be removed by taking partial hits into account using the return intensity. The scan density used (five to eight scans per 20 m by 20 m plot) was sufficient to ensure that occlusion of the laser beam was not significant. The choice of sampling density of the lidar data is important, but over a certain sampling density the gap fraction estimates become insensitive to further change. The lidar gap fractions altered by around 3%-8% when all subjective parameters were adjusted over their complete range.

The choice of manual threshold for the hemispherical photographs is found to have a large effect (up to 17% range in gap fraction between three operators). Therefore we propose that, as long as a site has been covered by sufficient scan positions and the data sampled at high enough resolution, the lidar gap fraction estimates are more stable than those derived from a camera and avoid issues with variable illumination. In addition the lidar allows the determination of gap fraction at every point within a plot rather than just where hemispherical photographs were taken, giving a much fuller picture of the canopy. The relative difference between TLS (taking intensity into account) and camera derived gap fraction was 0.7% for Abisko and -2.8% for Sodankylä with relative root mean square errors (RMSEs) of 6.9% and 9.8% respectively, less than the variation within TLS and camera estimates and so bias has been removed.

1 Introduction

The work presented here is part of a larger project which aims to improve numerical models used for weather and climate (Reid *et al.* 2013). Land surface models (LSMs) are used in general circulation models to make predictions of climate and water availability (Clark *et al.* 2011). Snow has a dramatic effect upon climate, but snow processes are a known weakness of LSMs, particularly in forests (Rutter *et al.* 2009). Part of this weakness comes from predicting snow melt over different land cover types that affect radiation balance and heat fluxes in different ways.

Radiative transfer (RT) schemes, which form a part of LSMs, model how forests interact with radiation (both long and shortwave) and how much reaches the snow, contributing to melt energy (Musselman *et al.* 2013). RT models with a range of complexities exist, but all struggle with validation. Complex models require vast amounts of data whilst simpler models subsume processes into effective parameters which are not directly measurable. In both cases it is difficult to determine whether the correct result is being reached for the right reasons (Widlowski *et al.* 2005) and so how transferable a model is.

A terrestrial laser scanner (hereafter referred to as lidar or TLS) is capable of measuring the full structure of a forest canopy in far more detail than any other practical method (Omasa *et al.* 2003, Jupp *et al.* 2009, Seidel *et al.* 2012). This allows the development of a complex radiative transfer (RT) model which can be used to test more efficient models for use in LSMs.

In this study we are primarily interested in capturing the effect of vegetation on light rather than in measuring the vegetation itself (although that is relevant to other applications) and so no attempt

was made to derive biophysical parameters such as plant area index (PAI). The most readily available method for validation is by comparison of gap fraction estimates against hemispherical photos (Bréda 2003, Danson *et al.* 2007). Validation against directly measured canopy area is possible over small areas (Hosoi and Omasa 2007) but is very time consuming.

1.1 Background

A number of previous studies have used terrestrial lidar to characterise forest structure. Tree trunks are not too different from buildings and other solid surfaces that TLS has been developed to measure and there have been a number of papers reporting success in determining diameter at breast height (DBH) and biomass (Watt and Donoghue 2005, Tansey *et al.* 2009). The radiation regime beneath a forest is controlled by the canopy and this is a different problem, requiring the characterisation of many small elements clumped into larger structures (Chen and Cihlar 1995, Widlowski *et al.* 2005). The canopy must be characterised to determine the forest's effect on snowmelt.

Danson *et al.* (2007) used the proportion of a single hemispherical lidar scan's beams recording hits to the total number to determine PAI, in the same way as a hemispherical photograph (Jonckheere *et al.* 2005). They found that the lidar tends to underestimate gap fraction compared to a camera and suggest that this may be due to the laser beam width; a hit would be recorded for any gap smaller than the beam width. They conclude that a better understanding of the interaction of lidar and a forest canopy is needed before it can be relied upon.

Seidel *et al.* (2012) used a similar approach to Danson *et al.* (2007) but with the extra capability of predicting the gap fraction for any point within a canopy rather than just from the lidar origin. This introduces the extra complication of laser beam occlusion; beams will be blocked as they strike canopy elements, leading to fewer samples as distance from scan centres increases. The effect of this can be reduced by using multiple scans; Seidel *et al.* (2012) used between six and thirteen scans per forest plot, roughly 20 m by 20 m. They further corrected for occlusion by placing 3 cm cubes at each recorded return in the radiative transfer model. They report a similar issue to Danson *et al.* (2007) of much lower lidar than camera-derived gap fractions (a factor of 0.57 different), though they did not determine whether this was due to laser beam width or the choice of 3 cm cubes.

Rather than treating each lidar return as a solid hit that blocks all light, which can introduce errors when merging multiple scans as elements may move between scans due to wind and geolocation issues, increasing the apparent canopy cover, Hosoi and Omasa (2006) proposed splitting the scene into voxels (volumetric pixels) and using the ratio of beams recording hits to the total number of occlusion beams passing through each voxel, as the PAI. The initial study used multiple scans of individual small trees (1.6 m tall and 70 cm crown diameter) and compared PAI estimates to direct destructive sampling (Hosoi and Omasa 2006). This gave very good agreement but there would be little occlusion over such a small crown and the laser beam width would be very small at the close ranges used, giving little indication how this method would perform over larger forests stands. The same group applied this method to a natural forest (Hosoi and Omasa 2007), using six separate, very high resolution scans (three from the forest floor and three from 10 m above the ground) to cover an 8 m by 4 m section of canopy. The method has also been applied to woody material (Hosoi *et al.* 2013). Again their results were good, with only slight underestimates in PAI at the top of the canopy (total error of 9.5%), although with 38% errors in fine branch volume, but it is not practical to cover larger areas at this level of detail. Huang and Pretzsch (2010) used a similar voxel method with two separate scans of a single pine tree crown and reported lidar gap fraction underestimates compared to a camera similar to Danson *et al.* (2007).

Côte *et al.* (2009) proposed a method for extracting very detailed explicit forest models from lidar scans. This uses a semi-supervised approach and a library of expected tree shapes to grow a model tree to fit the lidar data. This has been successfully used in forests (Côté *et al.* 2012) but it is not yet practical for characterising larger areas, especially in dense stands with overlapping crowns.

In recent years two groups have started building lidars optimised for forest measurements (Douglas *et al.* 2012, Gaulton *et al.* 2013), the SALCA (Salford Advanced Laser Canopy Analyser) and DWEL (Dual Wavelength Echidna®Lidar) instruments; which overcome a number of issues by using full waveform and two wavelengths. SALCA and DWEL are still in development but DWEL's single wavelength predecessor, Echidna (Jupp *et al.* 2009), has been tested in the field. Echidna results so far have either lacked coincident PAI or gap fraction measurements for validation (Strahler *et al.* 2008) or else agreed poorly with camera-derived estimates (r^2 of 0.23-0.41 (Zhao *et al.* 2011)).

Area	Plot	Trees	Height	Mean gap fraction	Std. dev.	TLS scans
Abisko	AR1	Birch	2 m	0.94	0.31	5
Abisko	AR2	Birch	3 m	0.89	0.30	5
Abisko	AR3	Birch	5 m	0.61	0.25	7
Abisko	AR4	Birch	4 m	0.67	0.26	7
Sodankylä	SC	Pine	18 m	0.41	0.19	8
Sodankylä	SR1	Pine	9 m	0.73	0.26	6
Sodankylä	SR2	Pine	11 m	0.46	0.20	8
Sodankylä	SR3	Spruce	15 m	0.41	0.19	8
Sodankylä	SR4	Pine	20 m	0.51	0.21	6

Table 1: Site characteristics. Plot names follow Reid et al. (2013). Mean gap fraction and standard deviation are across ten hemispherical photographs per plot.

2 Methods

Whilst previous studies have shown that lidar can accurately measure leaf area in a relatively small, intensively scanned area (Hosoi and Omasa 2007), these did not test radiative transfer aspects. Previous studies which have tested lidar's ability to capture radiative transfer within a forest suggest that lidar underestimates the gap fraction (Danson *et al.* 2007, Huang and Pretzsch 2010, Seidel *et al.* 2012), which would lead to an underestimate of light reaching the ground. This paper determines gap fraction from TLS point clouds anywhere within a canopy, implementing new methods to overcome the previously reported errors. These were compared to hemispherical photography-derived estimates (which cannot themselves be considered entirely accurate (Jonckheere *et al.* 2005)) and the reasons for disagreement determined.

2.1 Field sites

Field data were collected during two winter campaigns at Arctic sites representative of high latitude forests (Reid and Essery 2013). The first, in March 2011, was to Abisko in Sweden (69.325^{o}N, 18.832^o), an area of patchy, polycormic birch forest between 2 m and 4 m tall. Leaves were off during the field measurements, giving very sparse canopies.

The second, in March 2012, was to Sodankylä in Finland (67.365^{o}N, 26.635^{o}E). This is an area of pine and spruce forest between 2 m and 20 m tall and as these are evergreen, canopies were much denser than at Abisko.

At each site, five plots were chosen to cover a range of canopy structures, from young, very sparse canopies through medium aged, dense and homogeneous canopies to older, denser more heterogeneous canopies. Plot characteristics are given in Table 1. Each plot was a 20 m by 20 m square with one axis aligned north. Unfortunately at one Abisko plot the hemispherical camera coordinates came out well below the geo-referenced TLS point cloud, making the data from this plot unusable. No other Abisko plots suffered from this GPS processing issue and the method was changed for Sodankylä so that GPS was not needed.

2.2 Hemispherical photographs

The collection and processing of the hemispherical photographs used here is described in Reid and Essery (2013). A Nikon Coolpix 4300 camera with a Nikon FC-E8 fisheye lens was used to capture ten images per plot, positioned in a regular pattern (a diamond around the plot centre). The resulting images had a resolution of 1704 by 1704 pixels. Images were taken on cloudy days so that the sky brightness was as homogeneous as possible.

Images were classified as gap or canopy by manually thresholding, using the blue and red channels separately to help differentiate the sky from forest canopy (Reid and Essery 2013). An automatic branch joining algorithm was used on Abisko images to connect free-flying birch branch elements resulting from non-homogeneous sky conditions and bright reflections from white birch bark (Reid and Essery 2013). This branch joining was not used on the needle-leaf canopies of Sodankylä.

Beam divergence	70 μrad
Beam spacing	1 mrad
Angular accuracy	60 μrad
Range accuracy	4 mm
Wavelength	532 nm
Maximum range	300 m
Scan time	approx 12 min
Zenith range	-135^o to +135^o
Operating temp	0^{o}C to 40^{o}C

Table 2: Leica C10 characteristics at medium resolution

2.3 Lidar data

A Leica C10 first return terrestrial laser scanner was used. This records the range and intensity to the first object detected and has the characteristics given in Table 2 (all canopy scans were made at medium resolution). The plots were covered by between five and eight separate scan positions, depending on plot density. One scan was done at each plot corner, one or two near the centre and, if the canopy was tall enough, one or two approximately 10 m south of the southern edge to capture elements likely to cast shadows within the plot. Scans were not rigidly gridded, their positions being chosen so that every side of a tree crown was clearly visible from at least one position in order to minimise occlusion. Six 4.5" (11.43 cm) and four 6" (15.24 cm) diameter spherical targets were spread around the area to provide tie points between scans. Leica Cyclone^{TM} software was used to unify the scans with sub-centimetre accuracy.

The Leica C10 has a minimum operating temperature of 0^{o}C. In the air temperatures experienced (between -16^{o}C and 3^{o}C, typically around -6^{o}C) we found that the instrument would not work if powered down and up again. Therefore the instrument was kept on between scans.

2.3.1 Co-registration

At Abisko, a Trimble differential GPS was used to measure the camera and plot corner locations. The plot corners were visible in the lidar scans, allowing a transformation between coordinate systems to be calculated and the camera locations determined in lidar coordinates. At Sodankylä, a target was placed at each camera location, giving its exact position within the lidar point cloud. These temporary targets had their locations recorded by the TLS but were removed before the canopy scans were made.

2.4 Analysis software

To perform the initial comparison of lidar data to hemispherical photographs, the lidar point clouds were converted into hemispherical images using ray tracing. A silhouette ray tracer was used, tracing from each point to the camera rather than the more traditional tracing from the camera and performing intersection tests on the object (Disney *et al.* 2000). This is much more computationally efficient when the illumination source is irrelevant and multiple scattering can be ignored. This allows an estimate of the light regime at any point in the canopy from any number of lidar scans and is similar to that used by Seidel *et al.* (2012).

For this comparison to photographs, the ray tracer was used to produce synthetic, hemispherical, black (canopy) or white (gap) images from lidar data at each real camera location. Rather than a cube of constant size, as used by Seidel *et al.* (2012), a sphere with the same diameter as the inter-beam spacing at that range was put at each recorded return. Using the inter-beam spacing rather than the laser beam diameter ensures complete coverage but assumes the sampled areas are representative of obscured, unsampled areas. There is no way to avoid this assumption, except to set the beam spacing and divergence to the same value (not possible with the Leica C10). This ensures that areas far from a scan origin, where the laser beams are widely spaced, are compensated for by having larger spheres. Initial tests using the Monte-Carlo ray tracer of Lewis (1999) and sparse, leaf-free birch forest models of Disney *et al.* (2010) suggest that this variable sphere size gives accurate gap fraction estimates from the scan centre out to at least 20 m.

Each return casts a shadow on the synthetic image of its solid angle, taking into account range between the image origin and object and object size, to produce an image of gap or canopy. This was written in C and takes approximately 75 s to trace an image with 74 million points. The synthetic camera resolution can be set to any value and, unless otherwise stated, was set to 2924 (number of pixels across

a hemispherical diameter). The synthetic images generated from TLS are black (canopy) or white (gap) whilst the camera images have a range of brightness values that are later thresholded. Therefore the real hemispherical image contains more information than the synthetic lidar image of the same resolution (though the TLS image resolution can be adjusted at will and TLS intensity can be taken into account), and so the lidar image resolution was set higher than the camera resolution (1704 by 1704 pixels).

2.4.1 Partial hits

Objects that do not fill the field of view will still register returns, but placing a sphere the diameter of the beam spacing at a partial hit would overestimate the canopy cover (Danson *et al.* 2007). The energy returned from partial hits will be related to the fraction of the field of view filled, $\frac{A_p}{A_{fov}}$; where A_p is the area of the object projected into the laser beam path and A_{fov} is the area of the field of view at that point. The return intensity, I_r, is given by:

$$I_r = I_0 f(r) \rho_e \Omega \frac{A_p}{A_{fov}} \tag{1}$$

where I_0 is the outgoing pulse intensity, $f(r)$ is the range (r) dependence (inverse square with an extra optics overlap function), ρ_e is the element single scattering albedo and Ω is the phase function (angular behaviour of reflectance, also called BRDF). These last two variables are wavelength dependent. For the Leica C10 the measured intensity is scaled between -2047 and +2048 (rescaled between 0 and 1 for this study). More detail on this lidar equation can be found in Baltsavias (1999), although with different variable names.

In order to determine sphere size from intensity, a scatterplot of return intensity against range was drawn. The brightest returns at any range will be due to full hits (ie $A_p = A_{fov}$) on the highest albedo targets at a near normal angle of incidence. A line was drawn through these brightest returns by hand (chosen from the scatterplots in a similar way to a soil line (Liang 2004)) and used to determine $I_0 f(r) \rho_e \Omega$. It is not possible to decouple these variables from the lidar data alone. The example for Sodankylä plot SR4 is shown in Figure 2.4.1. This gave:

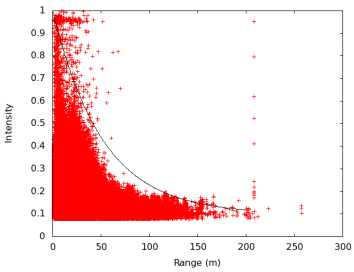

(a) Plot SR4

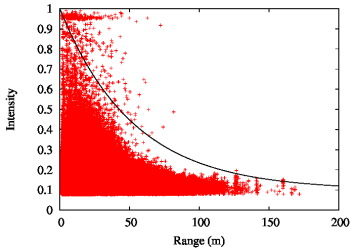

(b) Plot SC

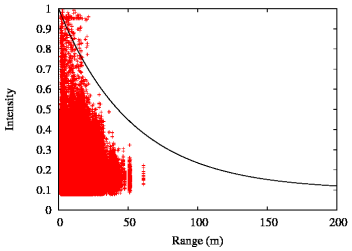

(c) Plot AR1

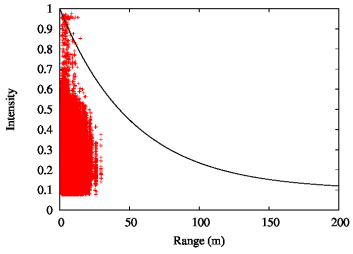

(d) Plot AR3

Figure 1: Scatterplot of return intensity against range for four example plots. The output intensity is scaled to lie between 0 and 1. All plots behaved similarly. Note Abisko plot point clouds were truncated at 50 m from scan centres.

$$I_0 f(r) \rho_e \Omega = 0.9 e^{-0.0195r} + 0.1 \tag{2}$$

This form was reasonable for all scans and sites (such as Figures 2.4.1 and 2.4.1), giving confidence in the instrument's stability. Note that, for Abisko, returns far outside the plot were removed during pre-processing and so Figures 2.4.1 and 2.4.1 show no returns beyond 40 m. Subsequent analysis concentrates on 70^o zenith and lower and so this removal does not affect later results. For each return, $\frac{A_p}{A_{fov}}$ can be calculated from the return intensity and used to scale the sphere diameter by substituting equation 2 into equation 1 and solving for $\frac{A_p}{A_{fov}}$;

$$\frac{A_p}{A_{fov}} = \frac{I_m}{0.9e^{-0.0195r} + 0.1} \tag{3}$$

where I_m is the intensity reported by the lidar (scaled to lie between 0 and 1). This provides a scaling factor for partial hits, though it will be an underestimate of sphere diameter for darker and non-normally oriented objects (tested in section 3.3.5), overestimating gap fraction but, conversely, we have no knowledge of the objects' location within the laser footprint and so can only place the sphere in the beam centre. This last factor could lead to an underestimate of gap fraction.

Synthetic hemispherical images were created with and without this intensity scaling to see how it affects the lidar underestimate of gap fraction reported by Danson *et al.* (2007), Huang and Pretzsch (2010) and Seidel *et al.* (2012).

2.4.2 Data storage

By default Leica Cyclone outputs an ASCII file of x, y and z position along with laser intensity and red, green and blue brightness from a coaxial camera. Due to the small size of canopy elements and slight breezes, the lidar and camera returns did not line up well; therefore the Leica camera data were rejected. In order to save space and speed up file reading (and so image generation) the ASCII files were converted into flat binary files in polar coordinates of range and laser intensity. Zenith and azimuth were implicitly given by location within the file (a header provides angular ranges and steps to allow this to be calculated).

This format was found to give smaller file sizes than directly converting the x, y, z and intensity data into a flat binary file. A typical ASCII file from a scan in Sodankylä was 413 Mbytes. The equivalent binary polar file was 85 Mbytes. The polar projection also made coarsening the data and identifying tree trunks (described in subsequent sections) easier.

2.4.3 Noise removal

Falling snow and spurious returns from the sun caused noise in the scans. In the denser forests, lower snowfall climate and cloudier skies of Sodankylä this was not noticeable, but in Abisko these returns caused noise in the synthetic hemispherical images. This was removed by splitting the point cloud into voxels, counting the number of points in each and rejecting all points in voxels containing less than a threshold number. A range of voxel sizes and thresholds was tested, with the results being assessed by examining synthetic images and videos. A voxel size of 20 cm and a threshold of 20 points was found to remove spurious returns above the canopy without deleting canopy returns. There will still be some snow returns within the canopy, but it is impossible to reliably remove these without first identifying the points from trees. At present this cannot be done except by complex, semi-supervised methods (Côté *et al.* 2012, Côte *et al.* 2009).

3 Results and discussion

The hemispherical photographs described in section 2.2 were collected in as near to ideal conditions as possible (uniform cloud or very low sun elevation and no precipitation). These were processed into black (canopy) or white (gap) images as described in Reid and Essery (2013).

The same plots were covered by between five and eight lidar scans. The lidar data were used to produce synthetic hemispherical gap-canopy images at the same locations and orientations as the real photographs. The subsequent sections compare these two sets of images and investigate the sensitivity of gap fraction estimates to a range of factors.

3.1 Initial comparison

Figure 2 shows hemispherical camera and lidar-derived gap images. They are recognisably of the same piece of forest, but there are a number of differences. The most obvious is that lidar shows more gaps

Sphere size	Unscaled		Scaled	
Site	Bias	RMSE	Bias	RMSE
Abisko	-2.2%	5.6%	0.7%	6.9%
Sodankylä	-8.1%	10.9%	-2.8%	9.8%

Table 3: Relative differences between lidar and camera-derived gap fractions for spheres of the beam spacing size (unscaled) and those scaled by return intensity.

at high zeniths (near the horizon). This is due to the limited range and occlusion of the lidar beam and so not detecting objects far from the plot centre. Hemispherical photographs measure the gap fraction out to infinity (the horizon). Seidel *et al.* (2012) noted the same effect and suggested that a lidar with a greater maximum range would overcome this. Their lidar had a maximum range of 79 m whilst the Leica C10 records up to 300 m; therefore even a quadrupling of maximum range has not solved the issue and occlusion must be the limiting factor. Note that in this snow covered, bright, landscape, the horizon sometimes had to be manually identified and masked in camera images; however due to range limits and occlusion this information is not recorded by the lidar at all.

The lidar sometimes shows fuller crowns than the camera, especially the tree in the centre of Figure 3.1. The lidar crown looks sensible and is unlikely to be spurious, therefore this is probably due to the camera missing canopy elements due to thresholding issues (Jonckheere *et al.* 2005) or blooming from bright clouds (Seidel *et al.* 2012). Other crowns seem fuller in the camera images than the lidar, for example the trees in the bottom right of Figure 3.1. This could be due to occlusion of the lidar leading to spurious gaps, the low resolution of the camera leading to spurious hits (Frazer *et al.* 2001) or optical aberrations in the camera (Wagner 2001).

The lidar shows gaps in the trunks of the two large trees in the centre of Figure 3.1. These gaps will appear in any solid object scanned from one direction and viewed from another and can only be solved (in this synthetic image from point cloud method) by fitting a solid surface to the points. Deciding which points are due to solid surfaces and which to porous is non-trivial, but a number of studies report success (Côte *et al.* 2009).

Geolocation issues could lead to errors in lidar/camera image alignment. These are more pronounced at low zeniths, where a small location error moves objects a larger angle than at higher zeniths. Therefore the low zeniths ($< 10^o$, chosen from graphs of gap fraction against zenith angle for all plots, such as figure 3.1) cannot be relied upon in direct comparisons. This was only an issue at Abisko where the GPS was used to register TLS and camera positions. At Sodankylä camera positions were measured by the TLS.

Figures 3.1 and 3.1 show comparisons of gap fraction estimates split by zenith (mean gap fraction along an annulus). The sphere size was not scaled by return intensity. The lidar gap fraction overestimate at high zeniths is clear (due to occlusion and limited range of the lidar), but otherwise the two follow a similar shape with slight differences. In subsequent analysis the average gap fraction (weighted by projected area) between 10^o and 70^o zenith was used to compare the methods in order to avoid issues of the lidar missing the horizon and geolocation. 70^o is also used as the cutoff in the LAI-2000 (LI-COR 1992) and allows a full characterisation of the canopy, if not the terrain. Unless otherwise stated, "gap fraction" refers to this weighted average for the rest of this paper.

3.2 Quantitative comparison

Figure 3.2 compares camera and lidar-derived gap fractions for all plots and camera locations using a sphere with the diameter of the beam spacing. The statistics are given in Table 3. The two estimates show good correlation, but the lidar tends to give a lower gap fraction. The error increases in denser canopies, which is to be expected as the more canopy there is the more chance there is for the different methods to disagree. This agrees with earlier findings (Danson *et al.* 2007, Huang and Pretzsch 2010, Seidel *et al.* 2012).

Figure 3.2 compares camera and lidar-derived gap fractions for all plots and camera locations, scaling sphere diameter by return intensity with equation 3. The relative errors (difference divided by the average of the two estimates) are given in Table 3. The lidar gap fraction estimate has been increased and is much closer to the camera estimate, thus scaling sphere sizes by intensity may have corrected for the laser beam width error identified by Danson *et al.* (2007). Abisko showed an increase in RMSE of 1.3% for a mean gap fraction of 76% with a standard deviation of 14%. It is not clear why the RMSE should increase, perhaps due to geolocation issues at Abisko, but it is not statistically significant. Note that the

(a) Lidar, Abisko plot AR4

(b) Lidar, Sodankylä plot SR4

(c) Photograph, Abisko plot AR4

(d) Photograph, Sodankylä plot SR4

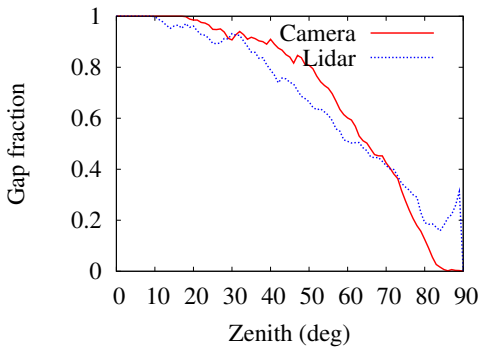

(e) Abisko plot AR4

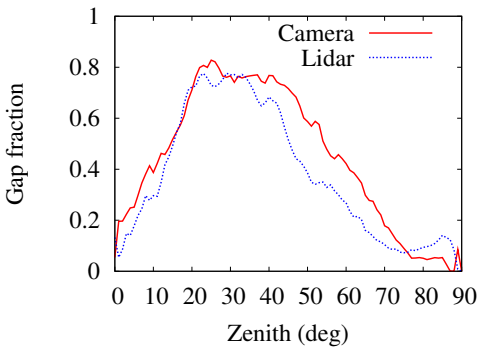

(f) Sodankylä plot SR4

Figure 2: Hemispherical gap fraction images from the camera and lidar. Intensity scaling was not used.

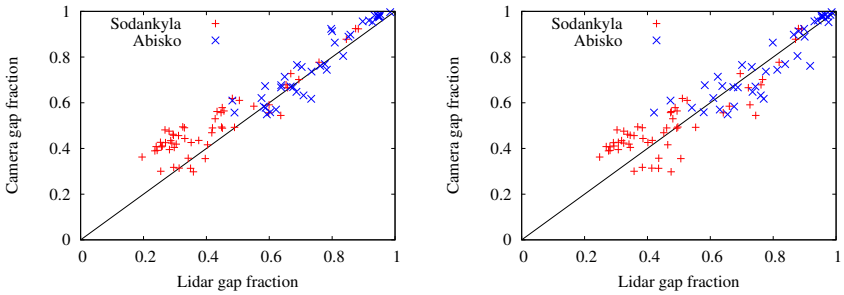

(a) (b)

Figure 3: Scatterplot of lidar and camera gap fractions for sphere sizes not scaled by intensity (a) and scaled by intensity (b).

camera estimates cannot be considered "truth" and so we cannot say for certain if the lidar estimate is now correct.

3.3 Sensitivity study

The lidar and camera gap fraction estimates are sensitive to a number of factors. For the lidar, the estimate depends upon the synthetic camera resolution, the scan resolution, occlusion of beams (controlled by forest density, scan density and scan position), the size of spheres (choice of scaling function in equation 3) and how solid targets are dealt with (gappy trunks).

The camera estimate depends upon camera resolution (Frazer *et al.* 2001), sky conditions and the manual thresholding. We have no control over the first two factors after the photo has been taken (though efforts were made to take photographs in optimal sky conditions) and the third is a subjective effect of the operator.

3.3.1 Camera threshold

Manually thresholding photographs to produce gap/canopy images is a subjective process (Jonckheere *et al.* 2005). Some automatic methods are available, but these still require local tuning to account for varied illumination conditions (Jonckheere *et al.* 2005). To assess the impact on gap fraction estimates, three operators independently thresholded the images from Abisko, where sky conditions were less homogeneous than at Sodankylä and so more challenging to threshold. For canopies with more than 10% canopy cover (<0.9 gap fraction), the spread in gap fraction estimates was of the order of 17% for the, harder, Abisko case. This is a significant spread, and purely from thresholding without any instrument or sky condition factors (Frazer *et al.* 2001), arguably suggest that gap fraction estimates from hemispherical photographs are more sensitive to subjective choices than is the case for lidar, despite the various factors discussed throughout this paper.

3.3.2 Synthetic resolution

Figure 4 shows the difference in lidar and camera gap fraction estimates against the ray tracer's resolution. Increasing the resolution decreases the lidar estimate, as gaps between objects are resolved (any pixel containing any part of an object is marked as canopy), until a plateau. Presumably this plateau occurs when every lidar return is resolved in the synthetic image.

The point at which this plateau is reached depends upon canopy density, with the curves for denser canopies plateauing later than sparser canopies. After the plateau we can be certain that the synthetic camera resolution is not affecting the gap fraction estimate, only the lidar characteristics and the choice of processing method (sphere size, surface fitting etc). A resolution of 8,000 pixels along a side was used for the rest of this study unless otherwise stated.

3.3.3 Occlusion

A first return lidar only measures up to the first object encountered; all objects behind this cannot be seen and so the beams are occluded as they pass through the canopy. We might expect areas with fewer

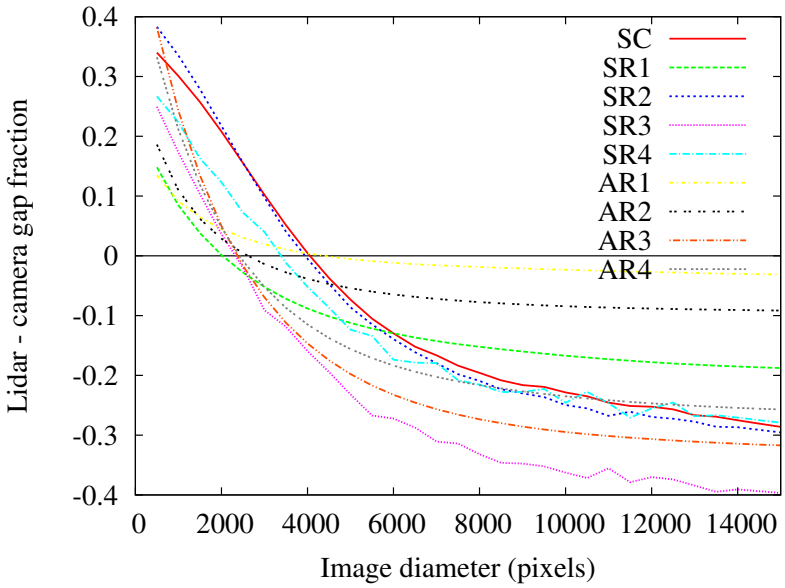

Figure 4: Difference between lidar and camera-derived gap fraction against synthetic lidar image diameter in number of pixels across the hemisphere

lidar beams passing through to have higher lidar gap fraction estimates relative to the camera. To test this, the number of lidar beams passing through each section of the canopy was determined and compared to the difference between the lidar and camera-derived gap fractions.

The plots were split into voxel cubes with sides of 50 cm. To save memory the voxels only covered a 60 m by 60 m (horizontal) by 18 m (vertical) area around the plot centre. This covers up to 70^o zenith for all camera positions and so does not limit accuracy in any way. The number of lidar beams from each scan position intersecting each voxel was recorded. If the beam had encountered an object before that voxel, a miss was marked, otherwise a hit was marked. From each camera position, rays were traced along the pixels of the hemispherical image, through the voxels and the total number of hits and misses counted. These were then binned into 5^o zenith and 20^o azimuth segments and the average number of hits and misses calculated. The lidar and camera-derived gap fractions were determined in these same segments, and the difference between the two plotted against number of hits.

If occlusion was having a significant effect we would expect the lidar estimate to increase relative to the camera estimate as the number of beams intersecting the voxel decreases. Scatterplots of the difference between TLS and camera derived gap fraction against the number of non-occluded lidar beams (figure not shown) showed no significant trend, therefore we conclude that the number and arrangement of scans used was sufficient to avoid occlusion in the areas of interest and so this is not contributing to the difference between lidar and camera gap fraction estimates. The results for Abisko may include geolocation issues, but that these results appear similar to those from Sodankylä suggests that this does not affect the results.

3.3.4 Scan resolution

The lidar scans were coarsened (sub-sampled) by aggregating adjacent beams (by an integer number only) and taking the first return within the group of beams as the object a coarser instrument would have recorded. These scans were then used to generate synthetic hemispherical images in the same way as above, approximating a broader beam divergence. A resolution of 11,000 pixels across a diameter was used, chosen based on Figure 4.

Figure 5 shows that for sparse plots (gap fraction >0.85) coarsening by even a factor of 9 causes no significant difference in the lidar derived estimate. For denser plots (gap fraction <0.85) coarsening causes an increase in gap fraction estimate. For the densest plot (SC) this increased from 0.65 to 0.84, an increase of 29%. For sparser plots this increase is less. This must be due to increased occlusion at coarser

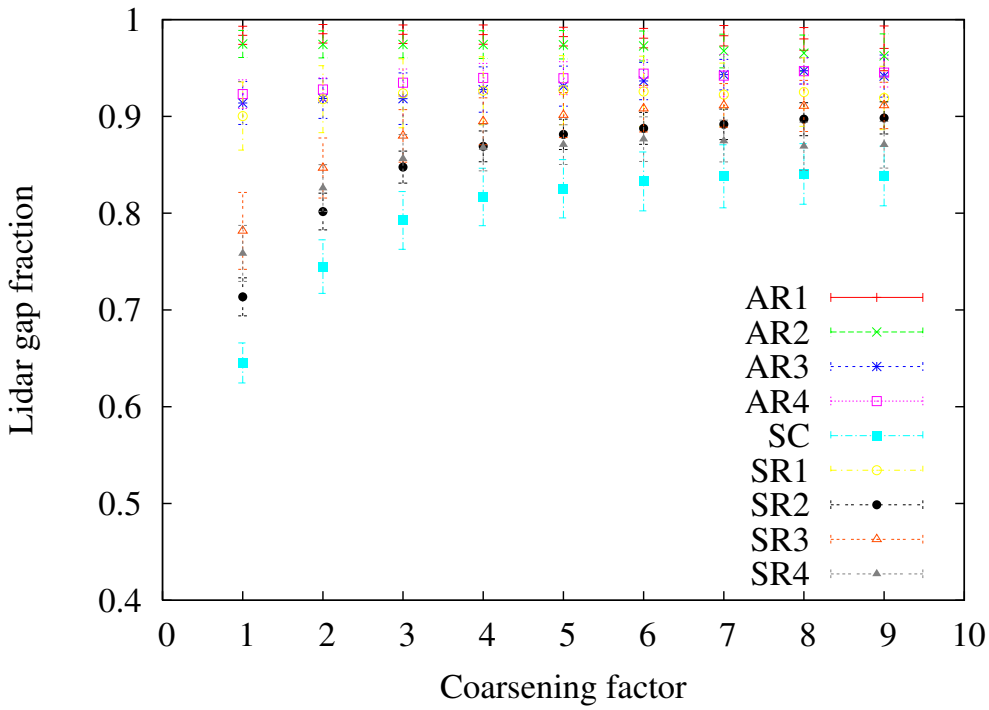

Figure 5: Mean lidar derived gap fraction against coarsening factors for each plot. Error bars show one standard deviation

resolution. Therefore scan resolution does have a significant impact in dense canopies. Section 3.3.3 suggests that the native resolution lidar data are not limited by occlusion, but these results suggest that a coarser resolution scan would have been. Thus care must be taken when choosing a lidar instrument for forestry work. Full waveform instruments will not suffer from the same occlusion issues. All visible elements are recorded rather than only the first, effectively giving an infinite angular resolution (in terms of occlusion only) and so the results may be less sensitive to scan resolution (Jupp *et al.* 2009, Hancock *et al.* 2007, Gaulton *et al.* 2013, Hancock 2010).

3.3.5 Sphere size

The sphere size set by equation 3 uses the reflectance of the highest albedo objects at a normal angle of incidence. All objects with lower albedos or higher angles of incidence will have their sphere size underestimated. To test this the scaling factor in equation 3 was divided by a factor between 0.1 and 1, representing the factor scaling between the highest and average combined albedo and phase function of the scene. The sphere size scaling factor was limited to 1 so that spheres cannot be larger than the beam spacing. The difference between lidar and camera-derived gap fractions was calculated for all camera locations and sites using these albedo factors. The results are shown in Figure 6. It should be noted that the phase function (angular dependence of reflectance) is wavelength dependent. At 532 nm reflection will be more specular than in the infra-red and so the Leica C10 may suffer a larger error than infra-red laser systems.

It can be seen that even when varying the average scene combined albedo and phase function between 10% and 100% of the brightest object, the final lidar gap fraction estimate only varied by 5%. There was no change for a mean combined albedo and phase function below 0.4; presumably because the sphere scaling factor reached 1 for all returns.

It may be possible to calculate the average scene albedo and phase function using a self calibrating method (Armston *et al.* 2013), but this effect seems to be small compared to other potential errors. The low sensitivity may be due to the fine beam spacing of the Leica C10 over the area of interest.

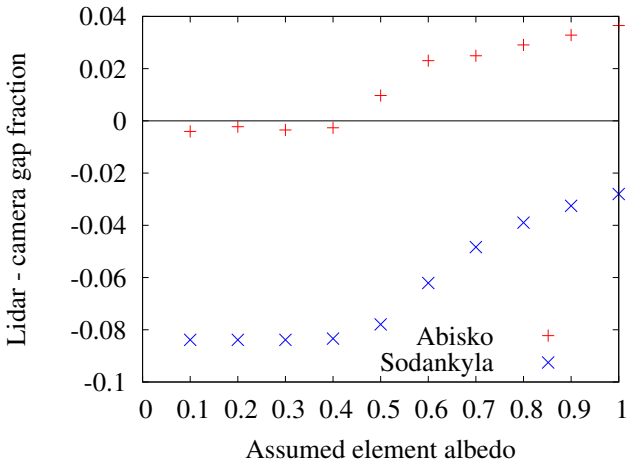

Figure 6: Difference between lidar and camera-derived gap fractions against assumed element reflectance and phase function as a fraction of the brightest

3.3.6 Large objects

Methods for fitting solid surfaces to trunks and branches exist, however they can be complex (Côté *et al.* 2012) and it is questionable whether any method would be robust in forests with such small, densely packed stems as Abisko, or with as much obscuring foliage as the Sodankylä spruce plot (SR3). Therefore no attempt was made to fit surfaces to trunks.

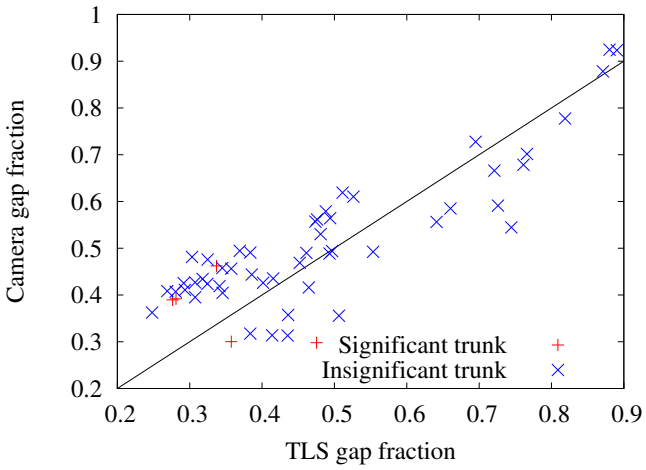

Figure 7: Camera against lidar-derived gap fraction separated by those with significant trunks and those without

If gaps in trunks were having a significant effect on the lidar gap fraction estimate, we might expect it to be lower than the camera estimate for images with large trunk areas than for images without significant solid objects. Figure 7 shows that this is not the case and so we can conclude that, for these forests, the trunks do not make up a large enough fraction of the canopy for the gaps between spheres to have a significant effect on the final value. It does lead to visually displeasing images however.

3.4 Limitations

A number of environmental factors may affect the lidar estimate, but there was not time to explore them in this project. Wind will move elements between scans and even between scan lines. From the point of view of a single scan, the gap fraction will not be affected as an element is as likely to be blown out of as into a beam path, but when looking from off the scan centre, or when merging multiple scans, the points will be spread over a larger area, decreasing the gap fraction. All scans used here were taken in low wind conditions, assessed subjectively by the operators. A quantitative assessment of their impact at different wind speeds and canopy types would be useful.

Snow and dust falling or being blown gave a noticeable number of returns. This was cleaned from the sky as described in section 2.4.3, but this would not remove any snow from within the canopy, where the point density is increased by genuine canopy returns. Scans were not made when fresh snow was falling, but even in light winds enough snow was carried to give some spurious returns. Comparing the gap fraction from one scan taken with no falling snow and another with falling snow would allow the impact to be quantified. The amount of falling snow can be quantified by the above canopy point density. Using an area of canopy covered equally by the two, such as a tree between two scan locations, would remove occlusion effects. There was not time to carry this out within the project. Snowflakes and dust are light and so are less of an issue for the camera, which interprets them as sky, if they are resolved in the image at all. Animals (especially insects) may be an issue in warmer areas.

This paper focused on gap fraction estimates and so the characterisation of the radiative transfer through the canopy. No attempt was made to extract plant areas index (PAI) or biomass as there was not enough time to collect data to validate (other than via gap fraction estimates, which suffer from their own issues (Chen and Cihlar 1995)). As Hosoi and Omasa (2007) have shown, PAI estimates with 9.5% error against direct measurement, can be achieved if enough separate scans are taken over a small area. It would be of interest to evaluate lidar's ability to evaluate PAI and radiative transfer simultaneously, ensuring that the correct forest biophysical parameters and light regimes are being reached for the right reasons rather than through empirically derived effective parameters (Widlowski *et al.* 2005).

4 Conclusions

Software for predicting gap fraction from terrestrial lidar data has been developed. This uses the intensity of TLS returns to overcome a previously reported limitation (Danson *et al.* 2007, Seidel *et al.* 2012). This is a "point cloud" method: Rays are traced from spheres placed at TLS return coordinates to a synthetic camera. This is much more computationally efficient than gap fraction or voxel methods (such as used to test occlusion in section 3.3.3) as each TLS return only needs to be interrogated once and no intersection tests are needed, saving computation time and RAM. The gap fraction estimates were compared to those from hemispherical photographs.

Using a high synthetic camera resolution on the lidar data, scaling the sphere size by return intensity and cleaning noise overcomes the previously reported gap fraction underestimate by lidar compared to hemispherical photography (Reid and Essery 2013). The lidar estimate is sensitive to the assumed combined element albedo and phase function and synthetic image resolution, but by equal or less than 5% in both cases, as long as the resolution is above a threshold, found to be 8,000 pixels in this study. Independently thresholded hemispherical photographs by three operators had a spread of 17% gap fraction at the harder Abisko site. Therefore we suggest that lidar is less sensitive to subjective choices than hemispherical photography in the majority of plots tested here. In addition the five to seven lidar scans per site allow the gap fraction to be predicted anywhere within the plot, not just at the ten camera locations and so give a much fuller picture of the radiative transfer.

Lidar's gap fraction estimate depends more strongly upon scan resolution for dense canopies, where occlusion is more significant. Therefore care should be taken when selecting an instrument for forestry work. Full waveform analysis may solve this problem without needing the large data files and scan times a higher resolution scan would cause (Jupp *et al.* 2009, Hancock *et al.* 2007).

The plots tested were well covered by lidar scans, ensuring that occlusion did not affect gap fraction estimates. Each plot took a full day to scan (scanning targets with high-resolution for registration was the most time consuming aspect), and required all four Leica C10 batteries available. A smaller number of scans may provide sufficient coverage and further tests of occlusion with variable numbers of scans would be useful.

Acknowledgements

This is part of a Natural Environment Research Council (NERC) funded project, grant number NE/H008187/1. S. Hancock was funded by the NERC National Centre for Earth Observation.

Thanks to the Abisko Naturvetenskapliga Station and the Finnish Meteorological Institute for hosting the team during fieldwork.

Thanks to Maya King, Cécile Ménard, Rob Holden, Mel Sandells, Mark Richardson and Milly Matthews-Mulroy for helping to collect the field data and to the two anonymous reviewers for their very helpful comments.

References

Armston, J., Disney, M., Lewis, P., Scarth, P., Phinn, S., Lucas, R., Bunting, P., and Goodwin, N., 2013, Direct retrieval of canopy gap probability using airborne waveform lidar. *Remote Sensing of Environment*, **134**, 24–38.

Baltsavias, E. P., 1999, Airborne laser scanning: basic relations and formulas. *ISPRS Journal of Photogrammetry & Remote Sensing*, **54**, 199–214.

Bréda, N. J. J., 2003, Ground-based measurements of leaf area index: a review of methods, instruments and controversies. *Journal of Experimental Botany*, **54**, 2403–2417.

Chen, J. M., and Cihlar, J., 1995, Plant canopy gap-size analysis theory for improving optical measurements of leaf-area index. *Applied Optics*, **34**, 6211–6222.

Clark, D. B., Mercado, L. M., Sitch, S., Jones, C. D., Gedney, N., Best, M. J., Pryor, M., Rooney, G. G., Essery, R. L. H., Blyth, E., Boucher, O., Harding, R. J., Huntingford, C., and Cox, P. M., 2011, The Joint UK Land Environment Simulator (JULES), model description - Part 2: Carbon fluxes and vegetation dynamics. *Geoscientific Model Development*, **4**, 701–722.

Côté, J.-F., Fournier, R. A., Frazer, G. W., and Niemann, K. O., 2012, A fine-scale architectural model of trees to enhance LiDAR-derived measurements of forest canopy structure. *Agricultural and Forest Meteorology*, **166**, 72–85.

Côte, J.-F., Widlowski, J.-L., Fournier, R. A., and Verstraete, M. M., 2009, The structural and radiative consistency of three-dimensional tree reconstructions from terrestrial lidar. *Remote Sensing of Environment*, **113**, 1067–1081.

Danson, F. M., Hetherington, D., Morsdorf, F., Koetz, B., and Allgöwer, B., 2007, Forest canopy gap fraction from terrestrial laser scanning. *IEEE Geoscience and Remote Sensing Letters*, **4**, 157–160.

Disney, M., Lewis, P., and North, P., 2000, Monte Carlo ray tracing in optical canopy reflectance modelling. *Remote Sensing Reviews*, **18**, 163–196.

Disney, M. I., Kalogirou, V., Lewis, P., Prieto-Blanco, A., Hancock, S., and Pfeifer, M., 2010, Simulating the impact of discrete-return lidar system and survey characteristics over young conifer and broadleaf forests. *Remote Sensing of Environment*, **114**, 1546–1560.

Douglas, E. S., Strahler, A., Martel, J., Cook, T., Mendillo, C., Marshall, R., Chakrabarti, S., Schaaf, C., Woodcock, C., Li, Z., *et al.*, 2012, DWEL: A Dual-Wavelength Echidna Lidar for ground-based forest scanning, In *Geoscience and Remote Sensing Symposium (IGARSS), 2012 IEEE International*, IEEE, pp. 4998–5001.

Frazer, G. W., Fournier, R. A., Trofymow, J. A., and Hall, R. J., 2001, A comparison of digital and film fisheye photography for analysis of forest canopy structure and gap light transmission. *Agricultural and Forest Meteorology*, **109**, 249–263.

Gaulton, R., Danson, F. M., Ramirez, F. A., and Gunawan, O., 2013, The potential of dual-wavelength laser scanning for estimating vegetation moisture content. *Remote Sensing of Environment*, **132**, 32–39.

Hancock, S., 2010, *Understanding the measurement of forests with waveform lidar*, Ph.D. thesis, University College London, http://eprints.ucl.ac.uk/20221/.

Hancock, S., Lewis, P., Muller, J.-P., and Disney, M., 2007, Using Monte-Carlo ray tracing to investigate the measurement of forest parameters with the Echidna laser scanner. *The International Archives of the Photogrammetry, Remote Sensing and Spatial Information Sciences*, **34**, Proceedings of 10th ISPMSRS.

Hosoi, F., Nakai, Y., and Omasa, K., 2013, 3-D voxel-based solid modeling of a broad-leaved tree for accurate volume estimation using portable scanning lidar. *ISPRS Journal of Photogrammetry and Remote Sensing*, **82**, 41–48.

Hosoi, F., and Omasa, K., 2006, Voxel-based 3-D modeling of individual trees for estimating leaf area density using high-resolution protable scanning lidar. *IEEE Transactions on Geosciences and Remote Sensing*, **44**, 3610–3618.

Hosoi, F., and Omasa, K., 2007, Factors contributing to accuracy in the estimation of the woody canopy leaf area density using 3D portable lidar imaging. *Journal of Experimental Botany*, **58**, 3463–3473.

Huang, P., and Pretzsch, H., 2010, Using terrestrial laser scanner for estimating leaf areas of individual trees in a conifer forest. *Trees*, **24**, 609–619.

Jonckheere, I., Nackaerts, K., Muys, B., and Coppin, P., 2005, Assessment of automatic gap fraction estimation of forests from digital hemispherical photography. *Agricultural and Forest Meteorology*, **132**, 96–114.

Jupp, D. L. B., Culvenor, D. S., Lovell, J. L., Newnham, G. J., Strahler, A. J., and Woodcock, C. E., 2009, Estimating forest LAI profiles and structural parameters using a ground-based laser called Echidna. *Tree Physiology*, **29**, 171–181.

Lewis, P., 1999, Three-dimensional plant modelling for remote sensing simulation studies using the Botanical Plant Modelling System. *Agronomie*, **19**, 185–210.

LI-COR, 1992, *LAI-2000 plant canopy analyzer instruction/operating manual*, LI-COR inc., Lincoln, Nebraska.

Liang, S., 2004, *Quantitative remote sensing of land surfaces* (Hoboken New Jersey: John Wiley & Sons, Inc.).

Musselman, K. N., Margulis, S. A., and Molotch, N. P., 2013, Estimation of solar direct beam transmittance of conifer canopies from airborne LiDAR. *Remote Sensing of Environment*, **136**, 402–415.

Omasa, K., Qiu, G. Y., Watanuki, K., Yoshimi, K., and Akiyama, Y., 2003, Accurate estimation of forest carbon stocks by 3-D remote sensing of individual trees. *Environmental Science & Technology*, **37**, 1198–1202.

Reid, T., and Essery, R., 2013, New methods to quantify canopy structure of leafless boreal birch forest from hemispherical photographs. *Open Journal of Forestry*, **3**, 70–74.

Reid, T., Essery, R., Rutter, N., and King, M., 2013, Data-driven modelling of shortwave radiation transfer to snow through boreal birch and conifer canopies. *Hydrological Processes*, DOI: 10.1002/hyp.9849.

Rutter, N., Essery, R. L. H., Pomeroy, J., Altimir, N., Andreadis, K., Baker, I., Barr, A., Bartlett, P., Boone, A., Deng, H., Douville, H., Dutra, E., Elder, K., Ellis, C., Feng, X., Gelfan, G., Goodbody, A., Gusev, Y., Gustafsson, D., Hellstrom, R., Hirabayashi, Y., Hirota, T., Jonas, T., Koren, V., Kuragina, A., Lettenmaier, D., Li, W., Luce, C., Martin, E., Nasonova, O., Pumpanen, J., Pyles, R., Sameulsson, P., Sandells, M., Schadler, G., Shmakin, A., Smirnova, T., Stahli, M., Stockli, R., Strasser, U., Su, H., Suzuki, K., Takata, K., Tanaka, K., Thompson, E., Vesala, T., Viturbo, P., Wiltshire, A., Xia, K., Xue, Y., and Yamazaki, T., 2009, Evaluation of forest snow processes models (SnowMIP2). *Journal of Geophysical Research*, **114**, D06111.

Seidel, D., Fleck, S., and Leuschner, C., 2012, Analyzing forest canopies with ground-based laser scanning: A comparison with hemispherical photography. *Agricultural and Forest Meteorology*, **154-155**, 1–8.

Strahler, A. H., Jupp, D. L., Woodcock, C. E., Schaaf, C. B., Yao, T., Zhao, F., Yang, X., Lovell, J., Culvenor, D., Newnham, G., *et al.*, 2008, Retrieval of forest structural parameters using a ground-based lidar instrument (Echidna®). *Canadian Journal of Remote Sensing*, **34**, S426–S440.

Tansey, K., Selmes, N., Anstee, A., Tata, N. J., and Denniss, A., 2009, Estimating tree and stand variables in a Corsican pine woodland from terrestrial laser scanner data. *International Journal of Remote Sensing*, **30**, 5195–5209.

Wagner, S., 2001, Relative radiance measurements and zenith angle dependent segmentation in hemispherical photography. *Agricultural and Forest Meteorology*, **107**, 103 – 115.

Watt, P. J., and Donoghue, D. J., 2005, Measuring forest structure with terrestrial laser scanning. *International Journal of Remote Sensing*, **26**, 1437–1446.

Widlowski, J.-L., Pinty, B., Lavergne, T., Verstraete, M. M., and Gobron, N., 2005, Using 1-D models to interpret the reflectance anisotropy of 3-D canopy targets: Issues and caveats. *IEEE Transactions on Geoscience and Remote Sensing*, **43**, 2008–2017.

Zhao, F., Yang, X., Schull, M. A., Román-Colón, M. O., Yao, T., Wang, Z., Zhang, Q., Jupp, D. L., Lovell, J. L., Culvenor, D. S., *et al.*, 2011, Measuring effective leaf area index, foliage profile, and stand height in New England forest stands using a full-waveform ground-based lidar. *Remote Sensing of Environment*, **115**, 2954–2964.